Snowflake Divertor as Plasma-Material Interface for Future High Power Density Fusion Devices.

V. A. Soukhanovskii 1), R. E. Bell 2), S. P. Gerhardt 2), S. Kaye 2), E. Kolemen 2), B. P. LeBlanc 2), E. T. Meier 1), J. E. Menard 2), A. G. McLean 1), T. D. Rognlien 1), D. D. Ryutov 1), F. Scotti 2), A. Diallo 2), R. Kaita 2), R. Maingi 3), M. Podesta 2), R. Raman 4), A. L. Roquemore 2)

1) Lawrence Livermore National Laboratory, Livermore, CA, USA
2) Princeton Plasma Physics Laboratory, Princeton, NJ, USA
3) Oak Ridge National Laboratory, Oak Ridge, TN, USA
4) University of Washington, Seattle, WA, USA

Email address of main author: vlad@llnl.gov

Abstract. Recent NSTX results demonstrate that the snowflake divertor (SFD) configuration may provide a promising solution for mitigating steady-state and transient divertor heat loads and target plate erosion, and project favorably to future fusion devices. In NSTX, a large spherical tokamak with high divertor heat flux ($q_{peak} \leq 15$ MW/m^2, $q_{\|} \leq 200$ MW/m^2), steady-state SFD configurations lasting up to 0.6 s (10 τ_E) were obtained using the existing divertor poloidal field coils. The SFD geometry significantly increased the plasma-wetted area, the parallel connection length, and the divertor volumetric losses compared to the standard divertor configuration. The SFD formation led to a stable partial detachment of the outer strike point otherwise inaccessible in the standard divertor geometry at $P_{SOL} = 3$ MW and $n_e/n_G \simeq 0.6-0.8$ in NSTX (n_G is the Greenwald density). Peak divertor heat fluxes were reduced from 3-7 MW/m^2 to 0.5-1 MW/m^2 between ELMs, and from 5-20 MW/m^2 to 1-5 MW/m^2 at peak times of Type I ELMs ($\Delta\ W/W$=7-15 %). H-mode core confinement was maintained albeit the radiative detachment, while core carbon concentration was reduced by up to 50 %. Additional divertor CD_4 seeding increased divertor radiation further. Based on the NSTX experiments, the SFD configuration is being developed as a leading heat flux mitigation technique for the NSTX Upgrade device. An edge transport model based on the two-dimensional multi-fluid code UEDGE favorably projects SFD properties to NSTX-U, showing a significant reduction of the steady-state peak divertor heat flux from 15 to about 3 MW/m^2 expected in 2 MA discharges with 12 MW NBI heating.

1. Introduction

The present vision of the tokamak plasma-material interface is an axisymmetric magnetic X-point divertor that enables intense heat and particle fluxes from the core plasma to be directed to a separate divertor chamber for special handling. The envisaged handling strategies include partitioning the SOL power P_{SOL} between inner, outer, lower and upper divertor targets, reducing parallel heat and particle fluxes using divertor volumetric loss processes and geometry, as well as reducing the heat flux deposited on the plasma facing components (PFCs) via increasing the plasma-wetted area A_w [1, 2]. The ITER divertor design, a closed divertor with tilted vertical targets and a partial radiative detachment of the strike points, represents an optimized standard divertor geometry based on experimental tokamak studies, theory and modeling developments over the last two decades [1, 2, 3]. However, for the proposed advanced tokamak (AT) and spherical tokamak (ST) based fusion nuclear science facilities (FNSF) [4, 5] and for the DEMO [6], the standard divertor solution is insufficient since the expected heat fluxes would exceed the presently allowed steady-state limit of 5-10 MW/m^2 and ELM-like transient limit of 0.1-0.5 MJ/m^2.

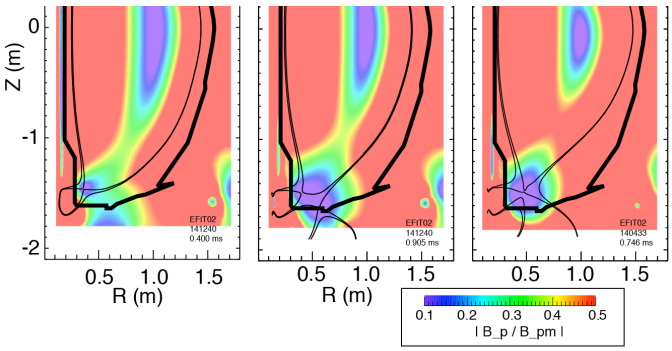

Figure 1: *Plasma equilibria and poloidal field modulus normalized to its outer midplane value $|B_p/B_{pm}|$ in NSTX discharges with the (a) standard divertor; (b) SF-minus and (c) ideal SF configurations.*

A recently proposed snowflake (SF) divertor configuration [7] is a promising

plasma-material interface (PMI) concept that addresses a number of outstanding boundary issues, with increasing support from TCV [8, 9], NSTX [10, 11, 12, 13] and DIII-D tokamak experiments. The SF magnetic configuration uses a second-order null-point created by bringing two first-order null-points of the standard divertor together [7, 14, 15, 16]. Poloidal magnetic flux surfaces in the region of the second-order null have hexagonal separatrix branches with an appearance of a snowflake. The presence of a second-order null point can affect pedestal MHD stability and transport inside the separatrix and in the divertor via a significantly broadened low B_p region surrounding the null-point (as shown in Fig. 1), which leads to increased magnetic shear inside the separatrix, as well as increased divertor plasma-wetted area, effective connection length and divertor volume.

Recent SF divertor studies performed in the National Spherical Torus Experiment (NSTX), demonstrate that the SF configuration may provide a promising solution for mitigating steady-state and transient divertor heat loads and target plate erosion, and project favorably to future fusion devices. NSTX is a large ST with a compact divertor, lithium-coated graphite target plates and high divertor heat flux ($q_{peak} \leq 15$ MW/m^2, $q_{\|} \leq 200$ MW/m^2). The problem of heat flux handling and material erosion is aggravated in the ST geometry due to the compactness of the divertor [17, 18], and the requirement of reduced collisionality (lower density n_e/n_G, where n_G is the Greenwald density) core plasma [19, 20]. At present, the NSTX facility is being upgraded to new capabilities to enable ST physics studies to advance the ST as a candidate for FNSF [21]. In the NSTX-U device [20], discharges with $I_p \leq 2$ MA, $P_{NBI} \leq 10$ MW, $n_e/n_G \simeq 0.5 - 0.8$, and up to 5 s duration are projected to produce steady-state peak divertor heat fluxes in the range 15-25 MW/m^2, thereby challenging thermal limits of divertor graphite PFCs [22]. The leading heat flux mitigation scenarios for NSTX-U are considered to be the SF divertor geometry and the impurity-seeded radiative divertor (RD) technique, a combination of which can be applied to both the lower and upper divertors.

2. Snowflake divertor studies in NSTX.

The SF divertor configuration was created in NSTX with existing divertor coils, and it was found to be compatible with high core and pedestal confinement and stability, while in the divertor, a significant heat flux reduction between and during ELMs, an increase of impurity radiation, and a radiative detachment of the outer strike zone were observed. The SF divertor studies were performed using highly-shaped slightly asymmetric ($drsep \simeq 6 - 7$ mm), $B_t = 0.45$ T, $I_p = 0.8$ MA, 4 MW NBI-heated H-mode discharges with the ion ∇B drift direction toward the lower X-point. The scrape-off layer (SOL) power of $P_{SOL} \simeq 3$ MW was estimated using the core power balance as in Ref. [23]. Lithium coatings evaporated on lower divertor graphite target plates in the amount 80-100 mg per discharge were used for wall conditioning and fuel inventory control.

Magnetic properties and control. One advantage of the SF divertor configuration is that it can be realized with an existing poloidal field coil set on a number of existing or planned devices [20, 24, 25, 26]. In NSTX, three existing lower divertor poloidal field (PF) coils were used to obtain steady-state SF configurations [11, 10, 12]. These coils were located at distances 0.20-0.35 m (or $(0.35 - 0.60)$ a_{minor}, where a_{minor} is the plasma minor radius) from the X-point, and operated with currents in 2-12 kA range, well below the safety margins.

The core plasmas with SF configurations had similar shaping parameters w.r.t. to those achieved with the standard divertor: the plasma volume ($V \simeq 12$ m^3) and elongation ($\kappa \simeq 2.2 - 2.4$) were unchanged, whereas the bottom triangularity was slightly reduced ($0.65 - 0.8$). Highly-shaped plasmas are the basis for high-confinement and stability advanced operating scenarios in the ST [19, 27].

Active magnetic control of the SF configuration is essential due to the topological instability of the ideal SF [7, 15]. Nontheless, experimental scenarios in NSTX demonstrated that

the SF configurations could be sustained with limited feedback control of the existing PF coils. Plasma equilibria modeling with a Grad-Shafranov equilibrium code ISOLVER guided the SF configuration development by providing approximate strike point positions and PF coil currents for the SF configurations on NSTX [10, 28]. Two SF scenarios were developed. In one scenario, plasma shape and wall clearences, as well as lower divertor strike point positions were feedback-controlled by the plasma control system (PCS) in real time [10, 28]. This scenario resulted in SF configurations with limited stability and duration [10, 11]. In another scenario that led to more stable SF configurations, plasma shape and wall clearences were controlled by the PCS, however, the divertor coil current waveforms were pre-programmed [12]. Both scenarios enabled steady-state comparisons of the SF and the standard divertor configurations, however, some drift of the SF parameters (e.g, the inter-null distance) could not be avoided. A fast numerical algorithm for null-point tracking and position control is being implemented in the PCS for active SF control.

An ideal SF with a second-order null, as well as slight deviations from it, known as SF-plus and SF-minus configurations [7, 15], were obtained in NSTX, as illustrated in Fig. 1 [10, 12]. The deviation from the ideal SF is described by the parameter $\sigma = d_{XX}/a_{minor}$, where d_{XX} is the distance between the null-points. In NSTX, the asymmetric SF-minus configurations with $\sigma \simeq 0.3 - 0.5$ were used to study pedestal characteristics and divertor heat flux mitigation between and during ELMs.

The SF magnetic properties predicted theoretically [7] have been confirmed in NSTX experiments. As shown in Fig. 1, a region of low B_p around the SF nulls is larger than in the standard divertor configuration, and it extends not only throughout the divertor separatrix branches (legs), but also deeper inside the separatrix (w.r.t. standard divertor). The asymmetric SF-minus configuration (Fig. 1 (c)), for example, showed an up to 50-75 % increase in $L_{||}$ and A_w (proportional to the poloidal flux expansion f_{exp}) in the outer strike point region. The inner strike point region was affected in a similar manner. The high f_{exp} region extended throughout 30-50 % of the SOL width λ_q, estimated to be $5 - 6$ mm [22].

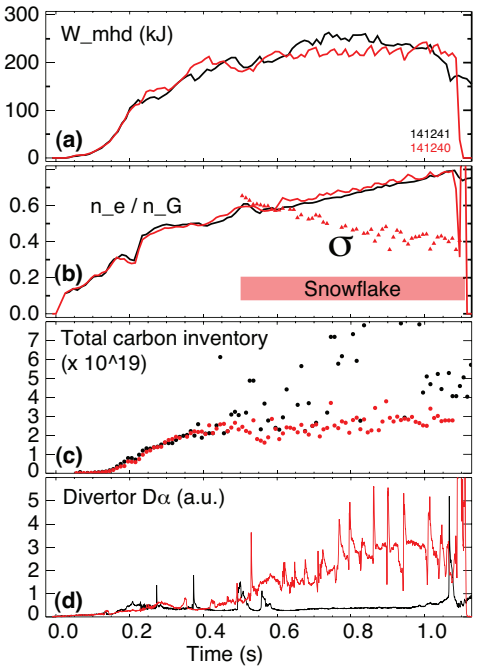

Figure 2: *Time traces of the H-mode discharges with the standard divertor (black) and SF (red): (a) Plasma stored energy W_{MHD}; (b) n_e/n_G and σ; (c) total carbon inventory N_C; (d) lower divertor D_α intensity.*

Core and pedestal properties. A second poloidal field null in the vicinity of the separatrix, or a second-order poloidal null, can affect edge turbulence, L-H power threshold and H-mode confinement characteristics via increased magnetic shear inside the separatrix and in the null-point region. This can also lead to stronger stabilization of ideal current-driven peeling modes and pressure-driven balooning MHD modes [14, 29, 30].

In NSTX, the SF configuration was compatible with high confinement plasma operation, with no degradation in H-mode core performance [10, 12] (Fig. 2). The SF configuration was realized at $n_e/n_G \simeq 0.6 - 0.8$. Core plasma parameters ($\bar{n}_e$, central $T_e \leq 1$ keV, $\beta_N \leq 4.5$) were similar to those in the 4 MW NBI-heated H-mode discharges with the standard divertor. Similar high performance metrics of these discharges, e.g., $\tau_E \simeq 50 - 60$ ms, $W_{MHD} \simeq 200 - 250$ kJ, and the factor H98(y,2)$\simeq 1$ calculated using the TRANSP code, confirmed minimal, if any, impact of the SF phase on confinement. In these high-triangularity plasmas, the L-H transition power threshold was fairly low (about 1 MW), therefore no H-mode threshold studies were performed. The SF divertor phase had a marked effect on plasma impurity content: the total carbon inventory N_c was reduced by 50-70 %. The observed reduction was attributed to the

reduction of carbon physical sputtering fluxes in the SF divertor (due to very low divertor T_e), and to the particle expulsion effect from ELMs that appeared in the SF phase [12].

The transition to the SF configuration in NSTX led to a clear and reproducible destabilization of ELMs. These large ELMs were classified as Type I, with somewhat irregular frequency of $f = 12 - 35$ Hz and $\Delta W_{MHD}/W_{MHD} \leq 15$ %. In the standard divertor H-mode discharge, lithium coatings on lower divertor PFCs reduced recycling and led to modified edge plasma pressure and current profiles and low-n peeling-ballooning mode stabilization [31, 32], as the pedestal stability operating point was close to the peeling boundary. Depending on the lithium conditioning and other operational factors, ELMs could be completely or partially suppressed. Understanding of the SF pedestal stability in NSTX is complicated by this and other factors, e.g., uncertainties in the electron pressure gradient and edge toroidal current density, as well as the plasma shaping changes (e.g. bottom triangularity) that accompanied the SF transition. In general, in the SF phase, the pedestal T_e was slightly reduced, while the pedestal n_e was also reduced due to reduced carbon density.

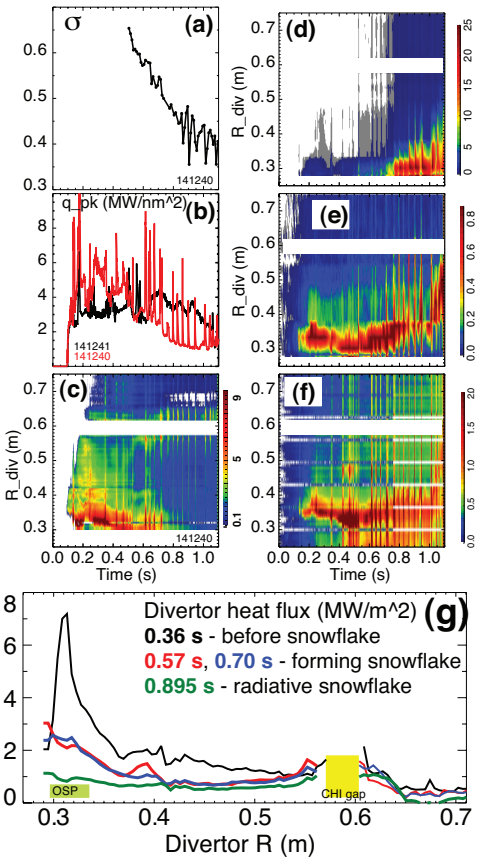

Figure 3: *Divertor time traces of the SF-minus discharge: (a) σ; (b) Peak divertor heat flux in the standard divertor discharge (black) and SF-minus discharge (red). Divertor contours of the SF-minus discharge: (c) heat flux; (d) deuterium $n = 6 - 2$ line brightness; (e) C III λ407 nm brightness (f) C IV λ581 nm line brightness; (g) Divertor heat flux profiles before, during, and after SF-minus formation).*

Steady-state divertor properties. The SF geometry had a marked impact on divertor properties in NSTX. A significant between-ELM reduction of divertor peak heat flux was measured [10, 12, 33, 9]. The SF-minus formation was always accompanied by a stable partial detachment of the outer strike point otherwise inaccessible in the standard divertor at $P_{SOL} = 3$ MW at $n_e/n_G = 0.6 - 0.8$ [17, 18] .

Fig. 3 illustrates the impact of the SF configuration on divertor heat flux and radiation. A detailed comparison with the standard divertor discharge was presented elsewhere [12]; here we discuss the properties of the SF-minus discharge. As the secondary null-point was formed and moved toward the primary X-point, the σ parameter was continuously reduced. The divertor volume, A_w, and $L_{||}$ were continuously increased, leading to large changes in divertor heat flux and radiated power. Additional volumetric losses were corroborated by the divertor carbon and deuterium Balmer-6 ($n = 6 - 3$) emission that also continuously increased, exceeding that of the standard divertor by up to 50 %. Divertor B6 line intensity is proportional to the electron-ion three-body recombination rate via the R/XB recombinations per photon factor (neglecting possible radiation trapping effects) [34]. During the SF formation period that lasted for 100-200 ms, divertor power decreased from 1.8-2.0 MW to about 1.2 MW, and the peak heat flux was reduced from 4-7 MW/m^2 to 2-3 MW/m^2 between ELMs. Brightness profiles of C III, C IV and B6 showed some broadening and also increased peaking in the primary X-point region. After the onset of detachment ($t \simeq 0.700$ s), q_{peak} further decreased to 0.5-1 MW/m^2, while the total power received by the outer divertor decreased to below 1 MW. The onset of detachment was accompanied by a further increase in the radiated power and volumetric recombination rate [12]. In spite of the formation of the highly-radiating detached region in the SF divertor, high core confinement was maintained for up to $10 \times \tau_E$ (i.e., up to a full duration of the SF phase 500-600 ms).

The heat flux reduction was interpreted as driven by both the geometric changes ($L_{\|}$, A_w) and the increased radiative and momentum losses. Shown in Fig. 4 are divertor geometry factors and peak heat flux between ELMs as functions of the σ parameter. Fairly clear trends can be seen albeit some data scatter. Note that the σ parameter was large ($\sigma \geq 0.6$, if meaningful) for the standard divertor, and the data for $\sigma \geq 0.65$ is not plotted. During the transition from the standard to SF geometry ($\sigma = 0.55-0.65$), divertor q_{peak} decreased concomitantly with increasing f_{exp} and $L_{\|}$. At $\sigma \leq 0.55$, a partial strike point detachment was observed, apparently driven by further increases in the SOL collisionality and volumetric losses from increased $L_{\|}$ and divertor volume.

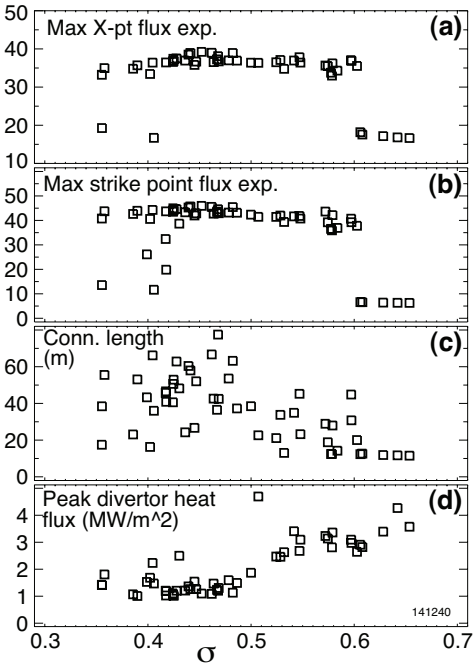

Figure 4: *Divertor geometry parameters and between-ELM peak heat flux as functions of σ: maximum f_{exp} in the (a) X-point and (b) outer strike point regions; (c) connection length $L_{\|}$; (d) peak heat flux.*

Impurity-seeded SF divertor operation. A significant reduction of steady-state divertor heat flux in the SF configuration is encouraging for future ST-based devices with inherently compact divertors. In previous NSTX divertor experiments, q_{peak} showed a linear scaling with P_{SOL} and a weak dependence on $n_e \simeq 0.5 - 0.8 \times n_e/n_G$ [18, 17, 22]. Partial detachment of the outer strike point was obtained in H-mode discharges with the standard (although high f_{exp}) divertor using additional extrinsic D_2 or CD_4 puffing [17, 18, 35]. The peak heat flux reduction in the SF configuration without gas seeding was similar to that measured in the the RD experiments using D_2 or CD_4 seeding at $P_{SOL} \sim 3$ MW. These results are summarized in Fig. 5.

The operational window of the gas-seeded RD at high P_{SOL} could be narrow as the required gas seeding rate could be incompatible with high pressure pedestal, ELM regime and X-point MARFE-free operation (e.g., [36]). In NSTX, additional CD_4 or D_2 seeding into the SF phase using a divertor gas injector showed excellent divertor gas screening from the core, increased divertor radiation, and stable MARFE-free operation (unaffected confinement) [35]. In the CD_4-seeded SF divertor, the divertor C III and C IV brightness profiles showed increased radiation, both in the intensity (i.e. due to the dependence of the carbon radiative cooling rate L_C on n_e, T_e), and in the spatial extent, due to the SF divertor high-flux expansion zone [35].

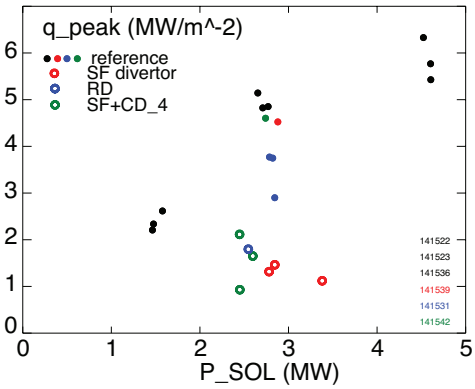

Figure 5: *Peak divertor heat flux q_{peak} as a function of scrape-off layer power P_{SOL} for the standard divertor discharges (filled circles) and the RD and SF discharges (open circles).*

ELM heat flux mitigation. Power partitioning due to heat diffusion between the separatrix branches and additional strike points in the SF configuration can be beneficial for steady-state divertor heat load handling, and perhaps even more critical for mitigating high transient heat and particle fluxes from Type I ELMs. Type I ELMs remain an unresolved issue for future divertor designs: ELM elimination techniques are explored, as radiative buffering of ELMs has been found ineffective [2].

Recent SF divertor theory and modeling developments highlight a number of SF effects on the transient ELM energy transport [16, 30, 37]. Reduced surface heating is expected due to the increased ELM energy deposition time τ_{ELM} and increased A_w as the ELM convective ion heat pulse with energy E_{ELM} travels over an increased field line length $L_{\|}$ connecting

the outer mid-plane to the divertor target. The surface temperature rise is given by $\Delta T \sim E_{ELM}/(A_w \times \sqrt{\tau_{ELM}})$. The second effect is the theoretically predicted convective mixing of the ELM heat in the null-point region leading to the heat flux partitioning between separatrix branches, and driven by the loss of MHD equilibrium, balooning modes and flute-like instabilities in the null-region [30].

In the NSTX asymmetric SF-minus configuration, the heat fluxes from Type I ELMs were significantly dissipated, as shown in Fig. 6, from about 5-20 MW/m^2 from an ELM in the standard divertor phase of the discharge, to 6-8 MW/m^2 during the SF formation phase and eventually below 2 MW/m^2 in the radiative SF phase. During the ELM heat pulse, the divertor plasma parameters (e.g., Balmer line intensities) showed signs of re-attachment. Peak target temperatures, measured by infrared thermography at peak ELM times, reached 1000-1200 ^{o}C in the standard divertor and only 300-500 ^{o}C in the SF phase. Apparent during ELMs was the emergence of an additional peak in the heat flux (and temperature) profile at the secondary separatrix location (and also where f_{exp} and L_X were close to those of the standard divertor). Assuming that radiation was not a significant ELM power loss mechanism, the ELM peak heat flux reduction was consistent with the theoretically predicted SF power sharing effects.

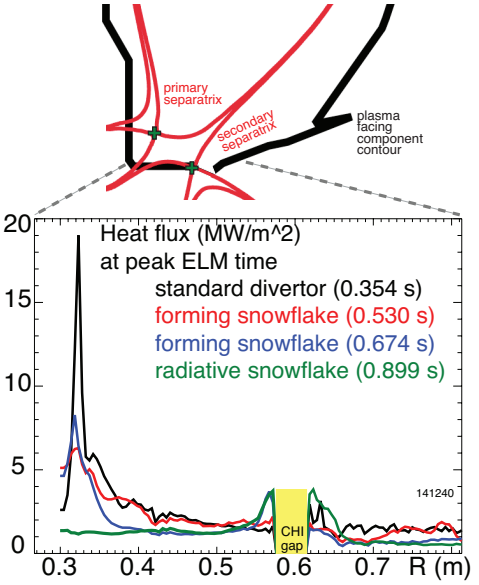

Figure 6: Peak divertor heat flux at peak ELM times before and during the SF formation, as well as in the radiative SF phase. The upper inset shows two separatrix branches in the asymmetric SF-minus configuration.

Peak ELM heat fluxes were reduced with increasing σ, in qualitative agreement with the theory of ELM heat transport trend with stronger SF effects (smaller σ) [30]. ELM measurements are summarized in Fig. 7. Plotted are the plasma stored energy loss due to ELMs ΔW_{MHD}, determined from equilibria reconstructions, and peak divertor heat fluxes for the few ELMs that occurred in the standard divertor phase, and in the SF phase. It should be noted that the heat flux in the inner divertor, that usually receives more heat during ELMs in tokamaks [1, 2, 3], was not measured in these experiments.

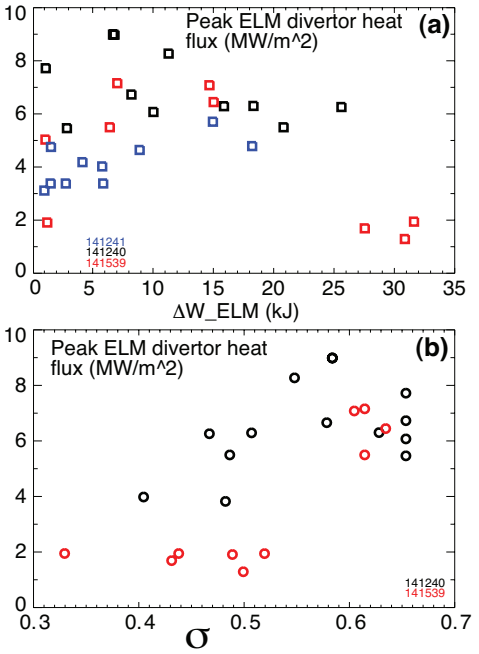

Figure 7: *Peak divertor heat fluxes measured at peak ELM times as functions of (a) the plasma stored energy loss due to the ELMs ΔW_{MHD} ; (b) the σ parameter.*

3. Modeling projections to NSTX-U.

One of the research mission elements of the NSTX Upgrade is the development of advanced PMI solutions toward FNSF/Pilot/DEMO [20, 21]. The SF divertor is a key element in this effort. Research is planned on NSTX-U to test SF magnetic feedback control, and demonstrate steady-state SF configurations with reduced heat flux, compatible with high-β, low collisionality H-mode scenarios [20].

To enable flexibility in divertor shaping control and SF configurations, an additional divertor coil is planned in NSTX-U, as shown in Fig. 8. Equilibria modeling was used to optimize the divertor coil layout. A number of magnetic equilibria with SF configurations have been modeled successfully using the predictive free-boundary Grad-Shafranov code ISOLVER (Fig. 8. Ideal SF, SF-minus and SF-plus configurations in the

lower an upper divertor regions could be realized with the up-down symmetric set of divertor coils operated below their respective current limits, and with plasma currents up to 2 MA. Four divertor coils should enable control of up to four independent parameters, e.g., positions of the null-points and strike points. A robust SF configuration sustainment was obtained in simulations even when time-varying leakage flux in the divertor region due to the time-evolving ohmic solenoid current was included [20]. In the SF-minus configuration shown in Fig. 8 , both A_w and $L_{\|}$ exceed those of the corresponding standard divertor by 50 %.

The modeled SF equilibria are used in predictive NSTX-U edge transport modeling with multi-fluid code UEDGE [38]. Initial results are summarized in Fig. 9. Comparative studies were performed between the standard and the SF-minus configurations. Numerical meshes spanning $0.9 \leq \psi_N \leq 1.05$ were generated. The geometric factors were very favorable for the SF-minus case: in the outer strike point region, $L_{\|} \simeq 20-30$ m (c.f. $7-15$ m in the standard divertor), and $f_{exp} \simeq 40-10$ (c.f. $10-20$ in the standard divertor. The divertor power balance was sensitive to the radial transport coefficients. In this set of simulations, $\chi_{i,e} = 1-2$ m^2/s and $D = 0.1-0.5$ m^2/s were used. A diffusive neutral model and a fixed fraction (5 % carbon) impurity model were used. In the model, ions recycled with $R = 1$ at the wall, and $R = 0.99$ at the divertor plates. The power flowing into the SOL was equally split between electrons and ions, and computations were performed over a range $5 \leq P_{SOL} \leq 9$ MW. The $P_{SOL} = 9$ case was representative of the 2 MA, 12.6 MW NBI-heated discharge. Total divertor heat fluxes and the heat fluxes without radiative heating are shown in Fig. 9. In the outer divertor region, high $q_{peak} \simeq 15$ MW/m^2 was obtained with the standard divertor, and only $3-4$ MW/m^2 in the SF configuration. The inner divertor region was found to be highly radiative (possibly with a detached strike point) in both configurations. The modeling provided a first encouraging look at heat flux mitigation in NSTX-U.

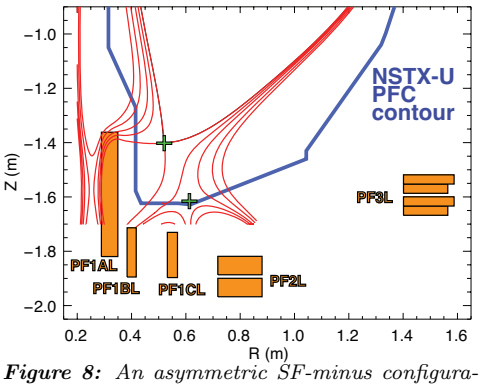

Figure 8: *An asymmetric SF-minus configuration modeled for NSTX-U divertor coil geometry. Flux surfaces separated by 1.5 mm in the midplane are shown. Near the separatrix, $L_{\|} = 38$ m and $L_X = 16$ m.*

4. Discussion and summary

Experimental results from NSTX, as well as the TCV and DIII-D tokamaks, support the SF divertor configuration as a viable divertor solution for present and future tokamaks. NSTX experiments demonstrated significant benefits of the SF divertor configuration, namely, steady-state and ELM divertor heat flux reduction via increased plasma-wetted area, volumetric losses, and power sharing between several strike points, as well as full compatibility with high-performance H-mode confinement and favorable edge stability modifications, in agreement with theory predictions. The SF divertor configuration apparently resulted in a reduced divertor temperature, which can have a positive impact on target material erosion as well as on seeded impurity radiation enhancement. Much experimental research is still needed to fully qualify the SF divertor configuration as a reliable candidate for future high-power plasma-material interface: real-time feedback control, edge pedestal MHD stability and ELM regimes, effects of 3D magnetic perturbations on the edge stability and divertor fluxes, and compatibility of the SF with divertor cryogenic pumping. The SF configuration is being developed as a leading divertor heat flux mitigation candidate for NSTX Upgrade [20], in support of the PMI development for the ST-based FNSF. Magnetic equilibria and edge transport modeling provide optimistic projections for handling divertor heat fluxes in NSTX-U discharge scenarios with plasma currents up to 2 MA, and NBI input power up to 12 MW. It is envisioned that all graphite PFCs as well as PFC conditioning via lithium and boron coatings would be used in the initial period of NSTX-U operation [20].

If NSTX-U divertor PFCs are upgraded to molybdenum, additional low Z impurity seeding combined with the SF divertor may become a necessity.

Acknowledgements We thank the entire NSTX Team for technical, engineering and computer support as well as plasma and diagnostic operations. This work was performed in part under the auspices of the U.S. Department of Energy under Contracts DE-AC52-07NA27344, DE-AC02-09CH11466, DE-AC05-00OR22725, W-7405-ENG-36, DE-FG02-04ER54758.

References

[1] ITER Physics Expert Group on Divertor et al., Nucl. Fusion **39** (1999) 2391.
[2] LOARTE, A. et al., Nucl. Fusion **47** (2007) S203.
[3] LIPSCHULTZ, B. et al., Nucl. Fusion **47** (2007) 1189.
[4] PENG, Y.-K. et al., Plasma Phys. Control. Fusion **47** (2005) 263.
[5] CHAN, V. et al., Nucl. Fusion **51** (2011) 083019.
[6] UNTERBERG, B. et al., Plasma-Wall Interaction Issues in DEMO, Submitted to J. Nucl. Mater. (2012).
[7] RYUTOV, D., Phys. Plasmas **14** (2007) 064502.
[8] PIRAS, F. et al., Phys. Rev. Lett. **105** (2010) 155003.
[9] CODA, S., Nucl. Fusion **51** (2011) 094017.
[10] SOUKHANOVSKII, V. et al., Nucl. Fusion **51** (2011) 012001.
[11] SOUKHANOVSKII, V. et al., J. Nucl. Mater. **415** (2011) S365.
[12] SOUKHANOVSKII, V. A. et al., Phys. Plasmas **19** (2012) 082504.
[13] SOUKHANOVSKII, V. A. et al., Advanced divertor configurations with large flux expansion, Submitted to J. Nucl. Mater (2012).
[14] RYUTOV, D. et al., Phys. Plasmas **15** (2008) 092501.
[15] RYUTOV, D. et al., Plasma Phys. Control. Fusion **52** (2010) 105001.
[16] RYUTOV, D. D. et al., A snowflake divertor: solving a power exhaust problem for tokamaks, Submitted to Plasma Phys. Control. Fusion (2012).
[17] SOUKHANOVSKII, V. et al., Nucl. Fusion **49** (2009) 095025.
[18] SOUKHANOVSKII, V. et al., Phys. Plasmas **16** (2009) 022501.
[19] GERHARDT, S. et al., Nucl. Fusion **51** (2011) 073031.
[20] MENARD, J. et al., Nucl. Fusion (At press, 2012).
[21] MENARD, J. E. et al., Progress on developing the spherical tokamak for fusion applications, in *Proc. 24th IAEA FEC, San Diego, 2012*, Paper FT/P3-4.
[22] GRAY, T. et al., J. Nucl. Mater. **415** (2011) S360.
[23] PAUL, S. F. et al., J. Nucl. Mater. **337-339** (2005) 251.
[24] RYUTOV, D. et al., in *Fusion Energy 2008 (Proc. 22nd Int. Conf. Geneva, 2008)*, CD-ROM file IC/P4-8, Vienna:IAEA.
[25] UMANSKY, M. et al., Nucl. Fusion **49** (2009) 075005.
[26] CALABRO, G. et al., Snowflake divertor plasma studies on FAST proposal, in *Proceedings of the 38th EPS Conference on Plasma Physics*, page P1.066, Strasbourg, France, 2011.
[27] GATES, D. et al., Phys. Plasmas **13** (2006) 056122.
[28] KOLEMEN, E. et al., Nucl. Fusion **50** (2010) 105010.
[29] UMANSKY, M. et al., Contrib. Plasma Phys. **50** (2010) 350.
[30] RYUTOV, D. et al., in *Proc. 24th IAEA FEC, San Diego, 2012*, Paper TH/P4-18.
[31] MANSFIELD, D. et al., J. Nucl. Mater. **390-391** (2009) 764.
[32] MAINGI, R. et al., Phys. Rev. Lett. **103** (2009) 075001.
[33] PIRAS, F. et al., Plasma Phys. Control. Fusion **51** (2009) 055009.
[34] TERRY, J. et al., Phys. Plasmas **5** (1998) 1759.
[35] SOUKHANOVSKII, V. A. et al., Divertor heat flux mitigation with impurity-seeded standard and snowflake divertors in nstx, in *Proceedings of the 39th EPS Conference on Plasma Physics*, page P5.049, Stockholm, Sweden, 2012.
[36] GIROUD, C. et al., Nuclear Fusion **52** (2012) 063022.
[37] RYUTOV, D. D., Contrib. Plasma Phys. **52** (2012) 539.
[38] ROGNLIEN, T. D. et al., J. Nucl. Mater. **196-198** (1992) 347.

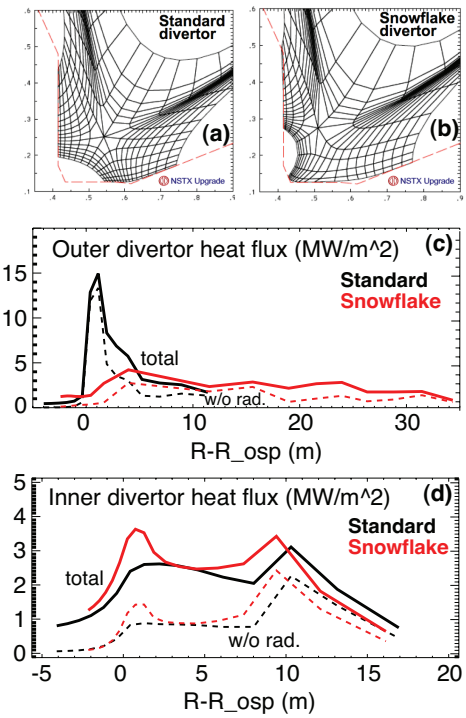

Figure 9: *UEDGE predictions for NSTX-U. Numerical meshes used in the models of (a) standard divertor and (b) SF-minus. Modeled divertor heat flux profiles in the standard divertor (black) and SF-minus (red) of the (c) outer divertor region; (d) inner (vertical target) divertor region. Solid lines show total heat flux, whereas dashed lines show heat flux excluding the radiative heating due to impurity radiation.*